Dynamic ion–ion and water–ion interactions in ion channels

Jin V. Wu
Department of Physiology, University of Rochester Medical Center, Rochester, New York 14642-8642 USA

ABSTRACT The dynamic interactions among ions and water molecules in ion channels are treated based on an assumption that ions at binding sites can be knocked off by both transient entering ions and local water molecules. The theory, when applied to a single-site model K^+ channel, provides solutions for super- and subsaturations, flux-ratio exponent (n') > 1, osmotic streaming current, activity-dependent reversal potentials, and anomalous mole-fraction behavior. The analysis predicts that: (*a*) the saturation may but, in general, does not follow the Michaelis-Menten relation; (*b*) streaming current results from imbalanced water–ion knock-off interactions; (*c*) $n' > 1$ even for single-site channels, but it is unlikely to exceed 1.4 unless the pore is occupied by one or more ion(s); (*d*) in the calculation involving two permeant ion species with similar radii, the heavier ions show higher affinity; the ion–ion knock-off dissociation from the site is more effective when two interacting ions are identical. Therefore, the "multi-ion behaviors" found in most ion channels are the consequences of dynamic ion–ion and water–ion interactions. The presence of these interactions does not require two or more binding sites in channels.

INTRODUCTION

The presence of ion–ion interactions within ion channels was demonstrated by the deviations from the independence relation in earlier studies (Hodgkin and Huxley, 1952; Chandler and Meves, 1965). More direct evidence was provided by the saturation behavior of single channel flux, which can be roughly fitted by the Michaelis-Menten relation (Hladky and Haydon, 1972; Horn and Patlak, 1980; Coronado et al., 1980). Reaction rate theory for channels with one binding site can be used to describe simple saturation if the enzyme conservation equation is adopted. This equation allows a binding site within the channel to be free or to be occupied by one ion. When an ion binds to the site, Coulombic interaction repels the incoming ions, thus making the site inaccessible. The use of this equation provides a simple way to include the effect of ion–ion interactions in channels. However, the result of these interactions in a pore differs from that of an enzyme. In ion channels, if the momentum of an incoming ion is large enough, a bound ion can be knocked off to the opposite side. The consequence of this process is a successful ion translocation from one side of the membrane to the other. The enzyme conservation equation includes only the outcome of the force exerted by a bound ion, but not the equal and opposite repulsion of the bound ion by incoming ions. This reactionary force facilitates the dissociation of the ion from the binding site to the *trans* side. Due to this inadequacy (a violation of Newton's third law), one-site rate theory fails to describe ion streaming as suggested by a flux-ratio exponent > 1. In the multi-ion Eyring rate theory, this difficulty is overcome by introducing additional binding sites; more ions can then be accommodated simultaneously by a channel (Hodgkin and Keynes, 1955; Heckmann, 1972; Hille and Schwarz, 1978). If the binding affinities are allowed to be varied with the occupancy state, the influence of repulsion exerted by incoming ions can be incorporated into the variation of these affinities. The multi-ion rate theory provides plausible explanations and quantitative fits for "multi-ion behaviors" (e.g., flux-ratio exponent > 1, the dual apparent binding affinities in saturation and block, and anomalous mole-fraction behavior) (Hille and Schwarz, 1978).

The overwhelming success of using multi-ion rate models to interpret experimental results has lead many investigators to propose that many types of channels can be simultaneously occupied by two or more ions (Hille and Schwarz, 1979; Begenisich and De Weer, 1980; Almers and McCleskey, 1984; Hess and Tsien, 1984; Eisenman et al., 1986; Bormann et al., 1987; Hill et al., 1989). This leads to the idea that channels may contain multiple binding sites. Furthermore, these permeation behaviors are accepted widely as structural criteria to identify multi-ion and multi-site channels. To interpret the complexity of ion permeation and block, there has been a growing temptation to suggest that a channel possesses even more binding sites. If these sites can be simultaneously occupied by several ions, with the constraints of long range Columbic repulsion among the bound ions, the narrow part of the channel must be fairly

0006-3495/92/05/1316/16 $2.00

long. Such a structure faces the following paradoxes. Firstly, the streaming potential in Ca^{++}-activated K^+ channels (K_{Ca}) suggests the narrow region of this pore is only 6–12 Å in length (Alcayaga et al., 1989). It is hard to visualize three or more K^+ ions with several water molecules lined up within this region. Secondly, it is often argued that these multi-occupancies might be stabilized by multiple negatively charged rings. However, the high conductance of K_{Ca} channels argues against this hypothesis, because multiple charged binding sites reduce the dissociation rate (Bezanilla and Armstrong, 1972). Thirdly, site-directed metagenesis of the voltage-dependent K^+ channel shows that the primary sequence of the constricted region is just eight amino-acids long, and only one of these amino acids is charged (Yellen et al., 1991). At this point, it would be incautious to claim a multi-ion channel before the following questions have been carefully examined. Do we have to increase the number of binding sites to fit experimental data? If we have to do so within the frame of Eyring rate theory, then can we find an alternative way to interpret the "multi-ion behaviors"? If such a theory can be developed, then how many binding sites are required for an adequate description of ion–ion interactions? In this work, I attempt to address these questions through a new approach in which the dynamic interactions among ions and water molecules are directly treated. To reduce the problem to its simplest terms, the analysis begins with a single-site model pore. The ion–ion interaction occurs when a second ion enters the channel transiently. It is shown in this work that the "multi-ion behaviors" can be explained by ion–ion and water–ion interactions. Their presence does not require two or more binding sites in a channel.

The peculiar "multi-ion behaviors" cannot be interpreted by one-ion rate theory. Analyzing these phenomena may provide a clue to understand the mechanism of ion–ion interactions. In selectivity studies, for example, the conductance ratio of a channel in symmetrical solutions is often surprisingly different from that of the permeability ratio determined by biionic reversal potentials. The permeation of K^+ and Tl^+ in a K^+ channel is intriguing due to the similar crystal radii (1.33 and 1.40 Å, respectively) of these ions. In symmetrical solutions, the conductance of K^+ is higher than that of Tl^+. In biionic solutions, however, the permeability of Tl^+ appears higher than that of K^+, as determined by reversal potentials (Eisenman et al., 1978, 1986). Although the higher K^+ conductance can be interpreted by higher average K^+ speed as a result of its smaller ion mass (m_K = 39.1 g/mol and m_{Tl} = 204.4 g/mol) (Wu, 1991), the higher Tl^+ permeability has not been given an unequivocal interpretation at the molecular level. It is generally inferred that the higher permeability of Tl^+ results from a higher binding affinity to a site within the channel (Eisenman et al., 1978; Yellen, 1987). If Tl^+ and K^+ bind to the same site, repulsions would prevent the larger Tl^+ from approaching the site as closely as K^+, and the electrostatic interactions will therefore be weaker in the former case. Thus, it seems unlikely that the high permeability of Tl^+ can result simply from binding. It is necessary to consider the role of ion mass. To show further the relevance of molecular weight to ion–ion interactions, the experimental result of Ba^{2+} current in a Ca^{2+} channel blocked by various divalent cations is summarized in Table 1 (Lansman et al., 1986). The concentrations in the second column are those that gave about the same degree of blockade of Ba^{2+} current. They approximately represent the inverse of the apparent binding affinity of the blocking ions. At first glance, the affinity is simply related neither to ion radius nor to ion mass. However, comparing affinities of ions with similar radii (Ca^{2+} and Cd^{2+}, or Mg^{2+} and Mn^{2+}), we find that a high apparent affinity is associated with high mass. Additional evidence that ion mass is involved in ion–ion interactions is given by the anomalous mole-fraction behavior in delayed rectifier K^+ channels (K_{DR}). The ability of ion X^+ (where X^+ = Tl^+, Rb^+, or NH_4^+) to block K^+ current when present in mixtures of X^+ and K^+, is in the sequence: $Tl^+ > Rb^+ > NH_4^+$ (Wagoner and Oxford, 1987). This sequence is consistent with their order of molecular weight. A similar pattern is observed in mixtures of X^+ and NH_4^+ in K_{Ca} channels, where X^+ = Rb^+ or K^+ (Eisenman et al., 1986). It is recognized in this work that ion mass is a major determinant in the dynamic interactions among ions and water molecules.

THEORY

Mechanism and qualitative descriptions of ion–ion and water–ion interactions

If an ion enters a channel and dwells at the binding site long enough, or the ionic activity is not too low, there is a significant probability that a

TABLE 1 Blockade of Ba^{2+}* current by divalent cations

Ion	Concentration for same degree of block of I_{Ba}	Ion radius‡	Ion mass
		Å	*g/mol*
Ca^{2+}	10 mM	0.99	40.1
Mg^{2+}	2 mM	0.82	24.4
Co^{2+}	250 μM	0.72	58.9
Mn^{2+}	100 μM	0.80	54.9
Cd^{2+}	20 μM	0.97	112.4

*Ba^{2+}: ion mass = 137.3 g/mol, ion radius = 1.34 Å.
‡Weast et al., 1989.

second ion will enter the channel and interact with the first. In the nanometer scale of known channel dimensions, the Coulombic long range interactions between these two ions cannot be avoided, even with the presence of a few water molecules between the ions. The interactions result in alterations of kinetic energy of both interacting ions. The consequence of long range repulsions on entering ions exerted by a bound ion can be simply included by using the enzyme conservation equation as in reaction rate theory. This equation ensures that, when the binding site is occupied by an ion, no additional entering ions can be allowed to bind to this site. To describe the effects of the reactionary force in which the bound ion is struck by entering ions, a more elaborate evaluation is needed. At the moment that an entering ion is interacting with the bound ion, the forces between these two particles are predominant comparing with the influences of the surrounding molecules. The kinetic energy may not be conserved in this process, but the ratio of the relative velocity before and after the collision is assumed to be a constant (e) according to Isaac Newton's experimental work (Cajori, 1934; Barnes, 1957),

$$V_A - V_B = -e(V_{0A} - V_{0B}) \qquad (0 \le e \le 1), \qquad (1)$$

where e is the coefficient of restitution; V_{0B} is the initial velocity of ion B at binding site; V_{0A} is the initial velocity of entering ion A; V_A and V_B are the velocities of ion A and B after an impact, respectively. Although the conservation of linear momentum of two interacting particles is questionable, it is reasonable to assume that the ratio of linear momenta after and before an impact (e') is a constant,

$$m_A V_A + m_B V_B = e'(m_A V_{0A} + m_B V_{0B}) \qquad (0 \le e' \le 1), \qquad (2)$$

where m_A and m_B denote the ion masses of ions A and B, respectively. Because Maxwellian velocity distributions of ion A and ion B are independent, to simplify the evaluation, one of them (V_{0B}) is represented by its average velocity. Thus, V_{0B} is considered to be zero at the binding site. Combining the above two equations gives the kinetic energy of the ion B at the binding site ($m_B V_B^2/2$) gained from the entering ion A,

$$E_B = \frac{m_A m_B}{(m_A + m_B)^2}(e' + e)^2 E_{0A}, \qquad (3)$$

where $E_{0A} = m_A V_A^2/2$ is the initial kinetic energy of an entering ion A. Define $\sigma = 4m_A m_B/(m_A + m_B)^2$ as ion–ion mass fraction of ions A and B. This parameter reflects the distinction of ion masses between two interacting ions, e.g., it equals 1 when the interaction is between two ions of the same species. Define $\delta = (e' + e)^2/4$ as the ion–ion energy transmission factor, i.e., the efficiency of the kinetic energy transferred from the entering ion to the bound ion. When $\delta = 1$, both kinetic energy and linear momentum are conserved, and energy transfer during a collision is maximal. The collision always reduces the velocity of the entering ion A ($|V_A|$ always $< |V_{0A}|$ in Eq. 1). After an impact between two ions, the ion B at the binding site gains energy from the entering ion A (E_B always > 0 in Eq. 3). Finally, the kinetic energy transferred from ion A to ion B is usually partial and is maximal only when the two ion masses are identical (Eq. 3). The above arguments may be extended to water–ion interactions. Define $\alpha = 4m_A m_W/(m_A + m_W)^2$ as the water–ion mass fraction for ion A, and $\beta = 4m_B m_W/(m_B + m_W)^2$ as the water–ion mass fraction for ion B, where m_W is the mass of a water molecule; also define $\mu = (e' + e)^2/4$ as the water–ion energy transmission factor.

For ion B to be dissociated from the binding site, its gained kinetic energy E_B through ion–ion knock-off interactions must be larger than its energy barrier W_B. According to Eq. 3, only those entering ions with kinetic energy $> E_B/\sigma\delta$ can knock off the ion B. The ion–ion knock-off rate of ion B by entering A ions is obtained by integrating the Maxwellian distribution (Wu, 1991),

$$\tfrac{1}{4} V_A S_B e^{-W_B/\sigma\delta kT}. \qquad (4)$$

When an ion binds to the site, another ion is allowed to enter the channel transiently and to interact with the bound ion. The kinetic energy of the entering ion is always reduced during the interaction (see Eq. 1). To exchange with the bound ion, this entering ion with reduced speed also has to overcome the dehydration barrier (W_{10} and W_{20}). Such transitions are negligible even when the ion mass of the entering ion is much bigger than that of the bound ion (see Appendix). From the mechanism of ion–ion and water–ion interactions proposed above, the following permeation behavior regarding ion–ion and water–ion interactions can be qualitatively interpreted.

(*a*) *Saturation.* The interaction between an ion at the binding site and incoming ions through Columbic repulsion decreases the kinetic energy of the latter. Therefore, the probability that they access the binding site is reduced. At higher activities, the probability of this self-block increases. The dwelling time of the ion at the binding site, or the apparent binding affinity of the site for the ion is expected to play a major role in determining the activity at which saturation occurs.

(*b*) *Ion streaming, water streaming, and flux ratio.* By obtaining enough kinetic energy in a collision, a bound ion at the site can be knocked off to the *trans* side. This results in a successful ion translocation. The higher the ionic concentration at the *cis* side, the more likely are the bound ions to be knocked off to the *trans* side. The extra ion translocations caused by this knock-off mechanism contribute to making the unidirectional flux-ratio exponent > 1. A similar mechanism can be extended to water streaming. If an osmotic gradient is applied across a channel, water molecules at one side have a higher probability of knocking off the bound ion than at the opposite side. The net translocated charges cause a streaming current, or a streaming voltage at equilibrium.

(*c*) *Reversal potential of ions with similar ion radii but different ion masses.* As an example, Tl^+ is placed in the bath, and K^+ is placed inside a cell, separated by a K^+ channel. If the independence principle were valid, K^+ efflux would be larger than Tl^+ influx. The positive reversal potential suggests that Tl^+ flux is actually higher than K^+ flux at zero current (Wagoner and Oxford, 1987). The interpretation from the present model includes the following two parts. Firstly, water–ion interactions are considered. According to the definition of water–ion mass fraction, $m_{Tl} > m_K$ results in $\beta(Tl^+) < \alpha(K^+)$. The smaller $\beta(Tl^+)$ increases the effective barrier height for this ion. In other words, once Tl^+ binds to the site, the dissociation rate of Tl^+ by water molecules is lower than that of K^+ in the same situation, i.e., Tl^+ stays at the binding site longer than K^+. Since Tl^+ is dissociated by water molecules at a lower rate, its affinity is apparently high. Secondly, ion–ion interactions are involved. For the situation of K^+ striking bound Tl^+ from the inside, because σ is only ~ 0.54, energy transfer is not effective, outward K^+ current is thus blocked by long dwelling Tl^+ at the binding site. For the situation of Tl^+ striking Tl^+ from the outside, σ is 1. Thus, Tl^+–Tl^+ knock-off interactions are effective for Tl^+ to be dissociated to the inside. For the same reason, K^+ at the binding site also blocks inward Tl^+ current. However, the longer duration of Tl^+ at the site reduces outward current more than the reduction of inward current by the binding of K^+. The net effect is a reduction of outward current or an increase in inward current at zero voltage.

(*d*) *Anomalous mole-fraction behavior.* In K^+ channels, the conductance in symmetric K^+ solutions is higher than that in symmetric Tl^+ solutions (Eisenman et al., 1986). If both solutions contain 10–40% Tl^+ with the remainder K^+, the conductance is unexpectedly lower than that in either K^+ or Tl^+ alone (Hagiwara et al., 1977; Wagoner and Oxford, 1987). Eq. 3 shows that the most effective knocking-off

impact occurs when the ion masses of the two colliding ions are identical. With a small amount of Tl^+ in K^+ solution, once a Tl^+ occupies the site, removal of block by either incoming K^+ or water molecules is not very effective, because only a small fraction of the kinetic energy of an incoming particle can be transferred to Tl^+. An increase in bath Tl^+ fraction provides more effective self-unblocking Tl^+ ions to knock off the bound ions of their own kind. This mechanism facilitates the current carried by Tl^+.

Quantitative descriptions of ion–ion and water–ion interactions: one ion species

For a channel with one physical binding site, the ion translocations across side 1 and side 2 can be illustrated by the following state diagram:

$$O + A_1 \underset{k_2}{\overset{k_1}{\rightleftharpoons}} OA \underset{k_4}{\overset{k_3}{\rightleftharpoons}} O + A_2,$$

where O is the binding site; A_1 and A_2 are the activities of ion A in side 1 and side 2, respectively. The flux equation of this process has the same form as that derived elsewhere through standard procedures of enzyme kinetics (Cleland, 1970; Hille, 1984):

$$j = j_1 - j_2 = \frac{k_1k_3A_1 - k_2k_4A_2}{k_2 + k_3 + k_4A_2 + k_1A_1}. \tag{5}$$

The difference between the current work and Eyring rate theory is that ions are allowed to enter the channel transiently and repel the bound ion. The entering ions are considered to bounce back after the interaction, and they therefore have no effect on the local energy profile of bound ions. The effects of these repulsions are described by dissociation constants of bound ions. As in the previous report (Wu, 1991), k_1 and k_2 are the rate constants for the ion A to pass over the compensated dehydration energy barriers. They are determined by the Maxwellian distributions of ions and can be expressed in terms of energy:

$$k_1 = \tfrac{1}{4} f_A V_A S_A e^{-W_{A10}/kT} \tag{6}$$

$$k_4 = \tfrac{1}{4} f_A V_A S_A e^{-W_{A20}/kT}, \tag{7}$$

where $V_A = (8kT/\pi m_A)^{1/2}$ is the average collision-free speed of ion A. It is a microscopic parameter and is different from the macroscopic ion speed, e.g., ion diffusion rate. S_A is the cross-sectional area of the selectivity filter. W_{A10} and W_{A20} are the energy barriers for ion A from side 1 and side 2 to the binding site, respectively. The ionic partition coefficient, f_A, is an adjustable constant (see Discussion). The dissociation rate constants, k_3 and k_4, are more complicated. The primary causes for ion A to be dissociated from the site O are the random motions of local water molecules and the long-range Coulombic interactions of entering ions. The water concentration of bulk solution is estimated by the following equation:

$$C_W^b = 55.51 - dA + gA^2 \quad \text{(mol/liter)}, \tag{8}$$

where d and g are constants for a given binary solute; they are obtained by evaluating published density and activity data. A is the ionic activity of the bulk solution. The water concentration within the channel interior is not clearly defined. A gross estimate of its dependence on ionic activities and channel structure is made possible by the following analysis. The water molecules in the bulk salt solutions may be conceptually placed into three categories: those associated with cations, those associated with anions, and those in the free state (Libuś, 1990). Because anions are excluded by an unfavorable entry energy barrier in cation channels, the portion of water molecules that are associated with anions is considered not to participate in intrachannel activities. The polar protein groups at the channel interior presumably substitute for a portion of the water molecules that associate with an entering cation during the dehydration process. Therefore, the water molecules within a channel are reduced by these two mechanisms. If this argument holds, the number of water molecules per unit volume within the channel can be estimated by

$$C_{wi} = f_W[55.51 - (d + h)A_i + gA_i^2] \quad \text{(mol/liter)} \quad i = 1, 2. \tag{9}$$

In this equation, h is the hydration number of an anion plus the number of water molecules with a cation that are substituted by the channel interior. f_W is an adjustable constant which can be interpreted as the partition coefficient of water in the channel. Using the knock-off rate derived in Eq. 4, the off-rate constants k_2 and k_3 can be expressed as

$$k_2 = \frac{S_a}{4}[f_A V_A A_2 e^{-W_{A01}/\delta kT} + C_{W2}V_W e^{-W_{A01}/(\alpha+c)\mu kT}] \tag{10}$$

$$k_3 = \frac{S_a}{4}[f_A V_A A_1 e^{-W_{A02}/\delta kT} + C_{W1}V_W e^{-W_{A02}/(\alpha+c)\mu kT}], \tag{11}$$

where V_W is the average speed of water molecules; S_a, the cross-sectional area of ion A; c, an adjustable mass-independent constant for water–ion interactions. W_{A01} and W_{A02} are the energy barriers for ion A from the energy minimum of the binding site to side 1 and side 2, respectively. Under the conditions of zero voltage and symmetrical pore, the unidirectional flux ratio can be obtained from the above flux equations and rate constants:

$$\frac{j_1}{j_2} = \frac{A_1[A_1 + (V_W C_{W1}/V_A)e^{-(1/(\alpha+c)\mu - 1/\delta)W_A^0/kT}]}{A_2[A_2 + (V_W C_{W2}/V_A)e^{-(1/(\alpha+c)\mu - 1/\delta)W_A^0/kT}]}, \tag{12}$$

where W_A^0 is the zero voltage energy barrier from the binding site to either side of a channel. Clearly, the flux-ratio exponent of this equation is between one and two. Thus, introducing the knock-off mechanism of ion–ion and water–ion interactions alone has demonstrated that a flux-ratio exponent > 1 can occur in a channel with a single binding site. If a channel contains a long and narrow region that only allows single-file ion movement (defined as a tunnel), the above equation for labelled ions is no longer true. This violation is illustrated in Fig. 1, where ions on each side are double-labeled as filled and open circles, respectively. They are separated by a channel with a long tunnel at each side of the selectivity filter. Assume that ion activities are sufficiently high to result in two ions in the tunnel of side 1 and one in the tunnel of side 2. The consequence of an "open circle" ion passing over the selectivity filter from side 2 to side 1 is a displacement of a "filled" ion out of the tunnel of side 1. Therefore, to translocate an "open circle" ion successfully across the whole channel from side 2 to side 1, three or more consecutive translocations across the selective filter from the same side are required. Following this theme and using a first order approximation, the flux-ratio for channels with a long tunnel can be estimated by

$$\frac{j'_1}{j'_2} = \frac{j_1}{j_2}\frac{[j_1/(j_1 + j_2)]^{n_2}}{[j_2/(j_1 + j_2)]^{n_1}}, \tag{13}$$

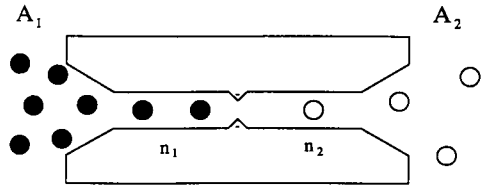

FIGURE 1 A schematic illustration of long tunnel effects on the flux ratio of double labeled ions. The narrowest part of the channel is the selectivity filter. The activity in side 1 (A_1) is much higher than that in side 2 (A_2). Here, an average of two ions are in side 1 of the tunnel (n_1), and one is in side 1 (n_2).

where n_1 and n_2 are the average numbers of ions in side 1 and side 2 of the tunnel, respectively.

Quantitative descriptions of ion–ion and water–ion interactions: two ion species

The ionic translocations involving two different ion species, A and B, can be represented by the following state diagram similar to that in reaction rate theory:

$$O + A_1 \underset{k_{2A}}{\overset{k_{1A}}{\rightleftharpoons}} OA \underset{k_{4A}}{\overset{k_{3A}}{\rightleftharpoons}} O + A_2$$

$$O + B_1 \underset{k_{2B}}{\overset{k_{1B}}{\rightleftharpoons}} OB \underset{k_{4B}}{\overset{k_{3B}}{\rightleftharpoons}} O + B_2.$$

The flux equation is derived through standard procedures of enzyme kinetics (Cleland, 1970; Hille, 1984):

$$j = \frac{\begin{array}{c}(k_{2B} + k_{3B})(k_{1A}k_{3A}A_1 - k_{2A}k_{4A}A_2) \\ + (k_{2A} + k_{3A})(k_{3B}k_{1B}B_1 - k_{2B}k_{4B}B_2)\end{array}}{\begin{array}{c}(k_{2B} + k_{3B})(k_{1A}A_1 + k_{4A}A_2) \\ + (k_{2A} + k_{3A})(k_{2B} + k_{3B} + k_{1B}B_1 + k_{4B}B_2)\end{array}}. \quad (14)$$

The flux represented by this equation is the time-averaged open single channel current. When two permeant ion species (e.g., K^+ and Tl^+) are present in the bath, the time constant for block by one ion species is calculated in the submicrosecond range (not shown in this report). If such fast blocking events cannot be resolved by contemporary recording systems, Eq. 4 is a good representation of the measured single-channel current.

The transitions from OA to OB and from OB to OA are omitted in the state diagram (see Appendix). The complication is again that a dissociation rate constant usually contains several contributions and depends on ionic activities. For example, k_{3A} contains three possible knock-off mechanisms: by water molecules, by ion A in side 1, and by ion B in side 1. These rate constants are derived as follows using previous procedures:

$$k_{1A} = \tfrac{1}{4} f_A V_A S_A e^{-W_{A10}/kT} \quad (15)$$

$$k_{1B} = \tfrac{1}{4} f_B V_B S_B e^{-W_{B10}/kT} \quad (16)$$

$$k_{4A} = \tfrac{1}{4} f_A V_A S_A e^{-W_{A20}/kT} \quad (17)$$

$$k_{4B} = \tfrac{1}{4} f_B V_B S_B e^{-W_{B20}/kT} \quad (18)$$

$$k_{2A} = \frac{S_a}{4}\left[f_A V_A A_2 e^{-W_{A01}/\delta kT} + f_B V_B B_2 e^{-W_{A01}/\sigma\delta kT} + C_{W2} V_W e^{-W_{A01}/(\alpha+c)\mu kT}\right] \quad (19)$$

$$k_{2B} = \frac{S_a}{4}\left[f_A V_A A_2 e^{-W_{B01}/\sigma\delta kT} + f_B V_B B_2 e^{-W_{B01}/\delta kT} + C_{W2} V_W e^{-W_{B01}/(\beta+c)\mu kT}\right] \quad (20)$$

$$k_{3A} = \frac{S_a}{4}\left[f_A V_A A_1 e^{-W_{A02}/\delta kT} + f_B V_B B_1 e^{-W_{A02}/\sigma\delta kT} + C_{W1} V_W e^{-W_{A02}/(\alpha+c)\mu kT}\right] \quad (21)$$

$$k_{3B} = \frac{S_a}{4}\left[f_A V_A A_2 e^{-W_{B02}/\sigma\delta kT} + f_B V_B B_2 e^{-W_{B02}/\delta kT} + C_{W1} V_W e^{-W_{B02}/(\beta+c)\mu kT}\right], \quad (22)$$

where f_A and f_B are the ionic partition coefficients (see Discussion). S_b is the cross-sectional area of ion B. A_1, A_2, B_1, and B_2 are the activities of ion A and B in side 1 and side 2, respectively.

The energy barriers in the rate constants above are calculated with the energy equation derived in previous work (Wu, 1991). The interaction energy between the bound ion and its nearest and next nearest neighbors in the region of the selectivity filter are specified as follows:

$$\begin{aligned} W(x) = &-\frac{QVx}{2L} + \frac{Q}{4\pi\epsilon_0}\left[\frac{q}{\sqrt{x^2 + R_p^2}} - \frac{q}{\sqrt{x^2 + R_n^2}}\right. \\ &\left. - \frac{p}{(L + a + b_{e1} + x)^2} - \frac{p}{(L + a + b_{e2} - x)^2}\right] \\ &+ \frac{qQ}{48\pi\epsilon_0}\frac{(a + b)^{11}}{(x^2 + R_n^2)^6} + \frac{pQ(a + b_W)^{10}}{24\pi\epsilon_0} \\ &\cdot\left[\frac{1}{(L + a + b_{e1} + x)^{12}} + \frac{1}{(L + a + b_{e1} - x)^{12}}\right]. \end{aligned} \quad (23)$$

The definitions of the symbols and the values of the parameters in this equation can be found in Table 2. Energy $W(x)$ was always minimized at $-L$ and L to ensure equilibrium at these two locations.

Parameter assignments and computations

The parameters used in this work fall into three categories. The first set, including ion radius, ion mass, and valence, is known. The second is unknown, but some of the parameters are in a range with certain constraints, e.g., the dimensions of the selectivity filter. The third group includes adjustable constants introduced within the theory. I attempted to use a single set of these latter constants for all cases. It was, however, much easier to fit the published experimental data if the parameters for the case of a single ion species and those for the case of two species are separately defined. This resulted in two sets of δ and μ shown in Table 2. The first set is for the solutions that contain only one cation species. The second set of parameters is used when two cation species are involved. The rest of the parameters are used consistently, unless indicated otherwise in Results. The d and g used in Eq. 9 are not listed in this Table. These constants were estimated through fitting the

published data to Eq. 8 (Robinson and Stokes, 1955; Weast, 1989). The obtained values of d, g are 3, 0 for KCl solution, 1.9, 0.14 for NaCl, and 11, 1.3 for sucrose. For the Tl^+, Rb^+, and NH_4^+ solutions, because no published data were available, d, g were all chosen to be 3, 0. In the case of two cation species in the solution, these constants from binary solutions are used without further corrections.

RESULTS

The energy profiles of K^+, Tl^+, and Rb^+ shown in Fig. 2 *A* were calculated from Eq. 25. A selectivity filter with axial-symmetrically arranged carbonyl groups was considered as a single physical binding site. The basic assumptions of this microscopic model are identical with those in previous work (Wu, 1991) except that the assumption of independence has been removed. The voltage across $L = -3$ Å and 3 Å is set at 1 mV. In Fig. 2 *A*, the first barrier from the left is highest for K^+ because its small radius results in the formation of a relatively tight hydration layer. The large central peak for Rb^+ is the consequence of the short range repulsions to its large radius. Some of these energy profiles show clearly two energy minima (O1 and O2), as a result of a combination of dehydration energy, potential energy of the binding site, and short range repulsions. Because these closely located minima (<2 Å) cannot be simultaneously occupied by two ions, they are treated as the fine structure of a single site as a first approximation. Therefore, only those knock-offs that cause the bound ion to jump over both barriers, e.g., from O1 to side 2 or from O2 to side 1, are considered. The two-step translocations from O1 to O2 then to side 2 or those in the reverse direction by two or more incoming ions are neglected (W_{01} and W_{02} include two barriers). Neglecting two-step jumps may cause an underestimation of the conductance of the ions with a large central barrier, e.g., Rb^+. Fig. 2 *B* shows the saturation behavior of K^+, Tl^+, and Rb^+ calculated from Eq. 5. The same set of parameters was used. The conductances shown in this figure are chord conductances with 1 mV across the selectivity filter. To establish a correct basis for the further discussion of ion–ion interactions among different ion species, it is desirable that the conductance sequences of K^+, Tl^+, and Rb^+ in symmetrical solutions be consistent with experimental results. The results of K_{Ca} channels are chosen as a comparison for this purpose, because more published results at the single-channel level are available. The conductance ratio is the secondary consideration. In Fig. 2 *B*, it fits with the experimental results reasonably well (Eisenman et al., 1986). The absolute conductances are less important with respect to this work. In addition to the consistency of Fig. 2 *B* with experimental results, two main features in this graph are worth mentioning as a lead for further investigations. Firstly, Tl^+ and Rb^+ saturate at much lower activities than K^+, which suggests that their apparent affinities are higher than that of K^+. This characteristic is experimentally observed in sarcoplasmic reticulum K^+ (K_{SR}) channels (Fox, 1983). Secondly, both Tl^+ and Rb^+ show a nonsaturable component at high activity. This behavior is found in K_{Ca} channels (Eisenman et al., 1986). The same component is noticeable also in the K^+ saturation.

TABLE 2 The set of parameters used for computation

Parameters	Descriptions	Value	Units
a_K, a_{Tl}, a_{Rb}	Ion radius of K^+, Tl^+, Rb^+	1.33, 1.40, 1.48‡	Å
b	Radius of carbonyl O	1.40	Å
b_W	Radius of water	1.56	Å
ϵ_0	Permittivity in vacuum	8.85×10^{-12}	farad/m
L	Distance for separation	3	Å
m_K, m_{Tl}, m_{Rb}	Ion mass of K^+, Tl^+, Rb^+	39.1, 204.4, 85.5	g/M
m_W	Mass of a H_2O molecule	18.0	g/M
p	Effective H_2O dipole moment	1.186×10^{-29}	Coulomb
q	Charge of carbonyl O or C	0.88 q_e*	Coulomb
Q	Charge of ion	1 q_e*	Coulomb
R_n	Distance of carbonyl O	2.88	Å
R_p	Distance of carbonyl C	4.18	Å
V	Voltage across $-L$ and L	1	mV
α	Mass fraction of H_2O & A^+	$4m_Am_W/(m_A + m_W)^2$	—
β	Mass fraction of H_2O & B^+	$4m_Bm_W/(m_B + m_W)^2$	—
σ	Mass fraction of A^+ & B^+	$4m_Am_B/(m_A + m_B)^2$	—
δ	Ion–ion energy transmission factor	0.6, 0.7	—
μ	Water–ion energy transmission factor	0.4, 0.25	—
c	Mass independent constant	0.5	—
f_W	Partition coefficient of H_2O	0.05	—
f_A	Partition coefficient of A^+	$(m_A/250)^{1/3}$	—
f_B	Partition coefficient of B^+	$(m_B/250)^{1/3}$	—
h	Number of H_2O with an anion + that replaced by channel	6	—

*$q_e = 1.6 \times 10^{-19}$ Coulomb, electron charge.
‡See Hille, 1984.

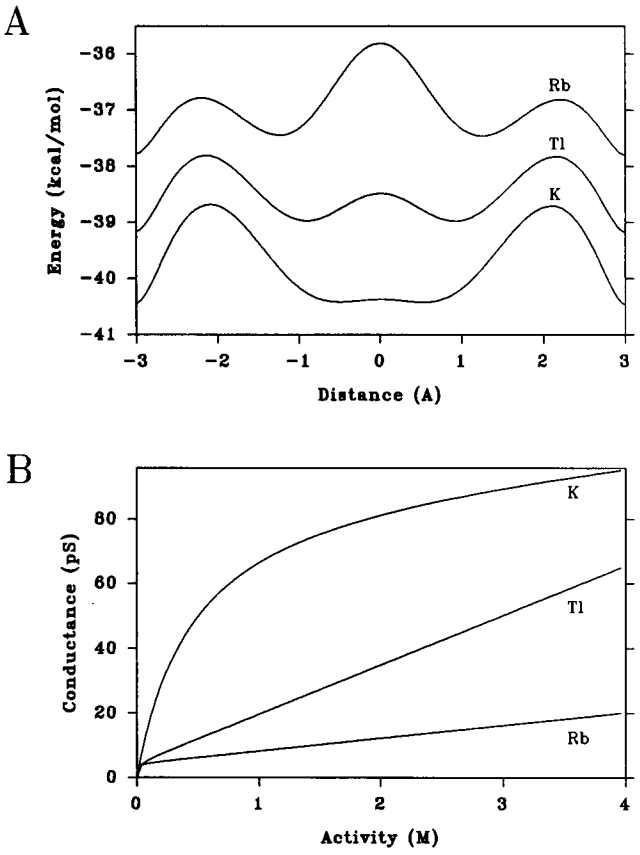

FIGURE 2 (*A*) The energy profiles of K^+, Rb^+, and Tl^+ in a hypothetical K^+ channel calculated from Eq. 23; 1 mV is applied across the selectivity filter. (*B*) The saturation behaviors of K^+, Rb^+, and Tl^+ calculated from Eq. 5. The energy profiles in *A* are used. The chord conductances are obtained at 1 mV.

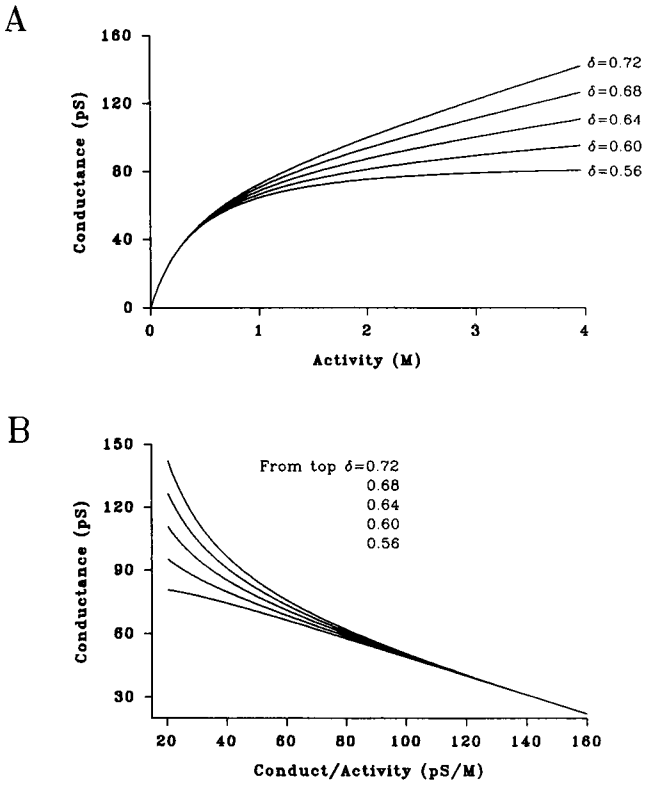

FIGURE 3 (*A*) Supersaturation behavior of K^+ with variation of the ion–ion energy transmission factor δ (values are labeled in the graph). (*B*) The Eadie-Hofstee plot of the curves in *A*.

Ion–ion knock-off interactions can produce supersaturation

To study the details of nonsaturable components of K^+ conductance, the ionic energy transmission factor (δ) is varied from 0.56 to 0.72. δ is defined as the efficiency of the energy transferred from an entering ion to the bound ion during an impact. All other parameters are identical with the set listed in Table 2. In Fig. 3 *A*, the nonsaturable component (defined as supersaturation) becomes progressively prominent as δ increases. The Eadie-Hofstee plots of these curves are shown in Fig. 3 *B*, as an assessment of the deviations from the Michaelis-Menten relation. These plots demonstrate that, at high activity, a larger δ results in more profound deviations from the Michaelis-Menten relation. Because δ is the dominant parameter found to alter the supersaturation, it is considered in this analysis that ion–ion knock-off interaction is a major cause of supersaturation. Conspicuous evidence for supersaturation has been found in hemocyanin channels (Latorre and Alvarez, 1981), acetylcholine receptor (AchR) channels (Dani and Eisenman, 1984, 1986), Na^+ channels (Green et al., 1989; Correa et al., 1991), large conductance K_{Ca} channels (Vergara et al., 1984), and K_{SR} channels (Coronado et al., 1980). The Eadie-Hofstee plots in these results show clear deviations from the linear relation of the Michaelis-Menten transformation. A common characteristic of these channels is that they belong to a category of pores with short tunnels (Cecchi et al., 1982; Dani, 1987; Begenisich and Busath, 1980; Alcayaga et al., 1989; Miller, 1982b). It is therefore suggested that supersaturation in these channels results from the more efficient energy transmission that may occur over shorter paths.

Subsaturation relates to water–ion knock-off interactions

In contrast to the supersaturation shown in some channels, the conductance of Gramicidin A (GA) channels (Hladky and Haydon, 1972), K_{DR} channels (Wagoner and Oxford, 1987), and sarcoplasmic reticulum Cl^-

channels (Hals et al., 1989) decline at high activity. These findings prompted further study to find out which parameter(s) determine(s) the falling phase of the saturation curve (defined as subsaturation). It turned out that h, the number of water molecules associated with an anion plus the cation-associated water molecules that are substituted by the channel wall, determines subsaturation. The saturation curves resulting from the variations of h are shown in Fig. 4 *A*. All other parameters are identical with the set listed in Table 2. These plots show that the extent of subsaturation increases when h is elevated. In Fig. 4 *B*, the Eadie-Hofstee plots of these data demonstrate deviations from the Michaelis-Menten relation. The interpretation of h as the determinant of subsaturation is twofold. Firstly, when cationic activity increases, the number of counter anions in the solution also increases, as does the number of water molecules associated with anions. These anions cannot easily enter a cation channel. Thus, those water molecules associated with anions are absent in water–ion knocking-off interactions. If the hydration number of an anion is high, a declination of conductance against activity may be prominent enough to be observable. The second consideration is dehydration by the channel lining. Because only the water molecules in the free state and those associated with cations can enter a channel to knock off the bound cation, the substitution of the cationic hydration layer by intra-channel polar groups reduces available water molecules in the channel. This point of view leads to a prediction that correlates channel structures. If the tunnel of a pore is long and polar, the number of water molecules in the channel may be substantially reduced. Then the probability of water–ion knock-off interaction decreases. There is structural evidence that the GA channel has a long tunnel (Urry, 1972). The flux-ratio exponent in K_{DR} channels ($\sim$3.3) provides reliable evidence that this channel has a long tunnel (Begenisich and De Weer, 1980). The above prediction can be extended further. Because removal of the hydration layer of a larger cation is easier, if a channel is permeable to several cation species and shows subsaturation, the larger cation is expected to exhibit more prominent subsaturation. This prediction is confirmed by the experimental results in GA channels in which Cs^+ shows more pronounced subsaturation than K^+ and Na^+ do at high activity (Hladky and Haydon, 1972).

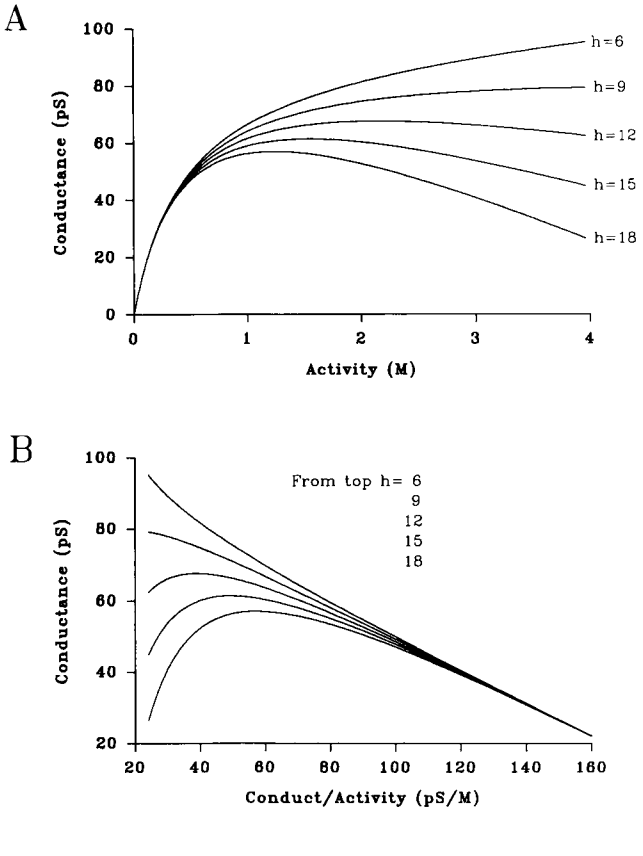

FIGURE 4 (*A*) Subsaturation behavior of K^+ with variation of the number of water molecules associated with an anion plus that of the cation-associated water molecules which are substituted by the channel lining (h). (*B*) The Eadie-Hofstee plot of the curves in *A*.

It is apparent that both supersaturation and subsaturation are present in these Eadie-Hofstee plots. With appropriate arrangement of f_W and f_A, the relative weights of ion–ion and water–ion interactions, a saturation curve can be very close to the Michaelis-Menten relation. Therefore, as a combined result of ion–ion and water–ion dynamic interactions, a saturation curve may, but in general does not, follow the Michaelis-Menten relation.

Half-saturation activity is determined by apparent affinity of the site

The apparent affinity of a site in this study is determined by three factors, the water–ion mass fraction (α), water–ion energy transmission factor (μ), and the energy barriers surrounding the site (W_{01} and W_{02}). The influence by the first of these can be partially shown in Fig. 2 *B*. The different ion masses of K^+, Rb^+, and Tl^+ lead to values of α_K, α_{Rb}, and α_{Tl}, equal to 0.86, 0.57, and 0.30, respectively. Despite the different energy profiles among these ion species, decreases in α for heavier ions (Tl^+ and Rb^+) are prominent enough to reduce their half-saturation activities. To avoid these effects of the different energy profiles and explicitly demonstrate the effect of the apparent affinity on half-saturation, the K^+

saturation curves are plotted by varying μ alone from 0.28 to 0.44, as shown in Fig. 5. Due to the presence of supersaturation, the curves with lower μ values exhibit two phases of saturation. The first phase is the Michaelis-Menton type of saturation resulting from repulsions of the entering ions by the bound ion. I define half-saturation as being associated with this phase. As μ decreases, the activity needed for saturation is significantly reduced. The second phase (supersaturation) results from ion–ion knock-off interactions and is independent of the first phase. The mechanism by which some heavy-metal ions potently block ion channels remains unknown. The most interesting examples are the two pairs of ions, K^+ and Tl^+, and Ca^{++} and Cd^{++}, whose radii, within each pair, are similar (Wagoner and Oxford, 1987; Kostyuk and Krishtal, 1977). The high apparent affinity of heavy ions has not yet been given a plausible interpretation at the molecular level. It is found in this work that the apparent affinity is closely related to the ion–water mass fraction (α and β). The more distinct the ion mass from that of water molecule, the harder for the ion to be knocked off from the binding site by water molecules; thus its affinity is apparently high.

Flux-ratio exponent relates to both ion–ion knock-off interactions and number of ions in the tunnel

If the tunnel of a pore is so short that any ions crossing the selectivity filter are considered to have escaped from the channel, the unidirectional flux ratio can be calculated from Eq. 12. The flux-ratio exponent, n', is then obtained from its definition. In Fig. 6*A*, n' is plotted against the activity at side 1. The activity at side 2 is kept as a constant, 100 mM. The voltage across the selectivity filter is 1 mV. The osmotic gradient-induced ionic flux was included in the calculation of n'. The curves in this graph correspond to three different δ values: 0.6, 0.7, and 0.8, respectively. The first feature of this plot is that n' is activity dependent. Raising the activity on side 1 increases the probability of ionic knock-off interactions, which leads to an increase in n'. The second feature is that an increase in the efficiency of knock-off (δ) promotes the increase in n' too. However, n' is not likely to exceed 1.4 by this mechanism, even with very prominent supersaturation. This finding shows that for a channel with only one physical binding site, n' can exceed one if ion–ion knock-off interactions are considered. The average n' for the Na^+ channel obtained from efflux tracer experiments is 1.03 (Begenisich and Busath, 1980), which falls into the range of n' discussed above.

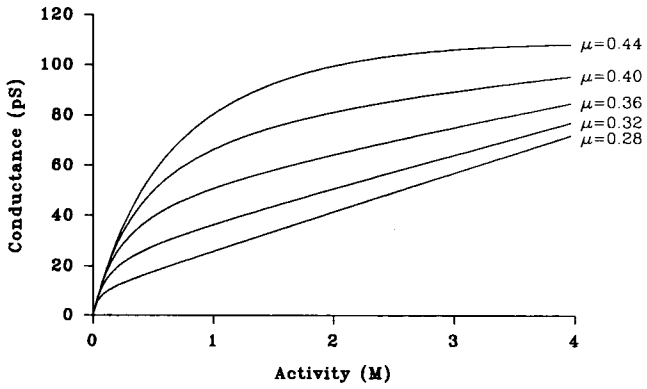

FIGURE 5 The behaviors of half-saturation with the variation of the water–ion energy transmission factor, μ.

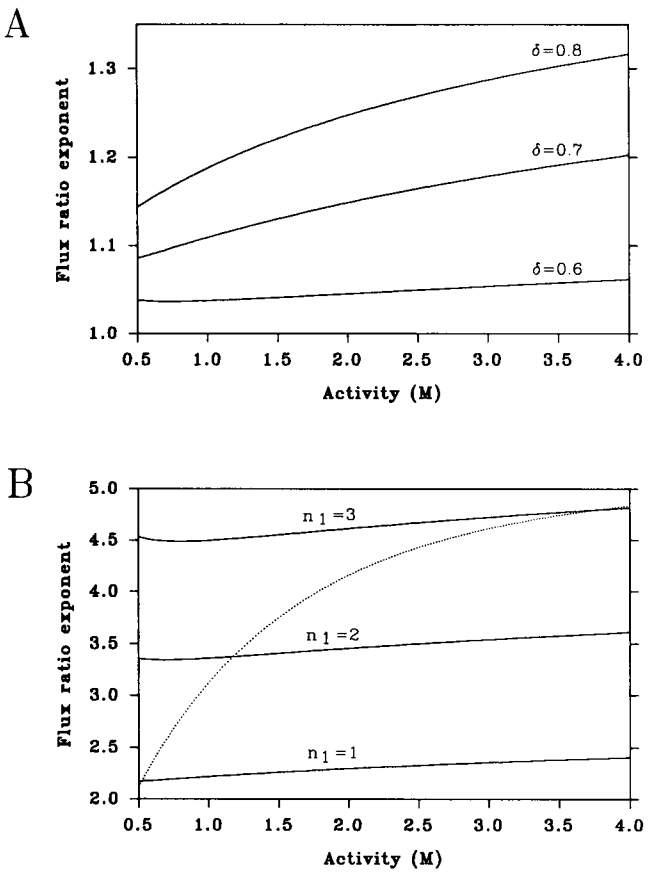

FIGURE 6 (*A*) The activity dependence of flux-ratio exponents (n') in a K^+ channel with a short tunnel. The activity in side 2 is 100 mM and that in side 1 is varied. The ion–ion energy transmission factors (δ) are labeled on each corresponding curve. (*B*) The activity dependence of n' in the K^+ channel with a long tunnel. The number of ions in the tunnel of side 2 (n_2) is 1 and that of side 1 (n_1) varies from 1 to 3. The dashed line is the fitted n', where n_1 is dependent on activity in the following way: $n_1 = 3.5[0.88 - \exp(-A_1/1000)]$.

Thus, the extracellular side of the tunnel in a Na^+ channel might be very short. This suggestion is consistent with the above predictions for supersaturation. The activity dependence of n' is in agreement with the results in inwardly rectifying K^+ channels (Spalding et al., 1981).

Fig. 6 *B* depicts the activity dependence on n' in channels with long tunnels, calculated from Eq. 13. The number of ions in the tunnel of side 2 (n_2) is 1, and that of side 1 (n_1) varies from 1 to 3. δ was chosen to be 0.70. The number of ions in the tunnel should not be considered as a constant through such wide range changes of activity. The dashed line represents a fit of n' in which n_1 is dependent on activity in the following way: $n_1 = 3.5[0.88 - \exp(-A_1)]$. We note from this graph that n' can reach 4.5 or even higher, if the tunnel is long enough to accommodate three or more ions. The n' is not very sensitive to n_2 (data not shown), if the activity in side 1 is much higher than that in side 2. Finally, it may be possible to estimate the average number of ions in the tunnel from experimental data of n'. For instance, since n' for K_{DR} channel can be up to 3.3 (Begenisich and De Weer, 1980), the average number of ions in the one side of the tunnel is estimated to be two from this analysis. However, such an inference should be made cautiously, because Eq. 13 is only an approximation. A more rigorous approach is required for a definitive evaluation.

Streaming current is a result of imbalanced water–ion knock-off interactions

Single channel *i*-V curves in symmetrical 300-mM K^+ solutions with varying sucrose activity are shown in Fig. 7. The current is calculated from Eq. 5. The reduction of free water molecules is estimated from Eq. 9 in which d and g are 11 and 1.3, respectively. The activity of sucrose indicated in the graph is added to the solution of side 2. If side 1 corresponds to the inside of the cell and side 2 is the outside, then the directions of current and voltage are consistent with conventional representations. As the sucrose activity in side 2 increases, the outward current is elevated progressively. The equilibrium potential becomes more negative. The presence of sucrose has two major effects on water concentrations. First, the sucrose in the solution displaces part of the water molecules in a unit volume of solution. Second, the hydration of sucrose reduces the amount of water molecules in the free state. The combination of these two effects is that the number of water molecules available in the channel to knock off the bound ions decreases. The difference in the probability of water–ion knock-offs between two sides causes a steady outward streaming current. Such streaming current and potential

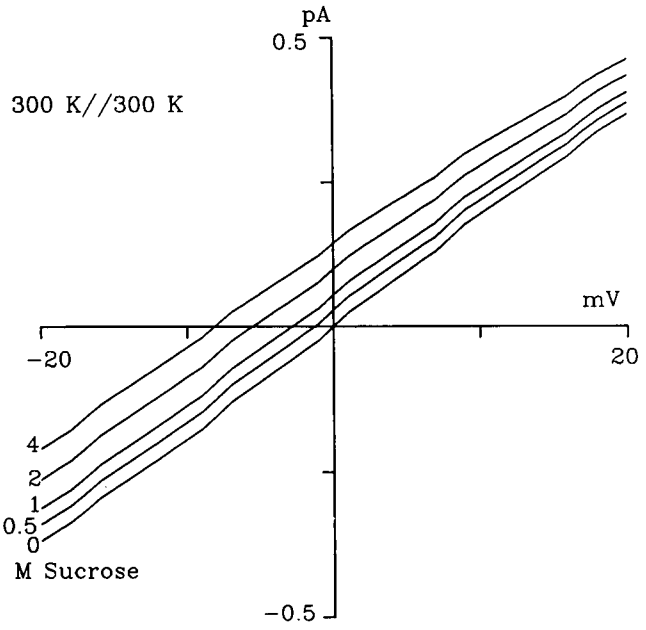

FIGURE 7 The osmotic gradient-induced shift of *i*-V curves. The curves correspond to 0, 0.5, 1, 2, and 4 M sucrose placed on side 2 of symmetrical 300-mM K^+ solutions. The direction of current flow from side 1 to side 2 is defined as positive.

have been observed in K_{Ca} channels (Alcayaga et al., 1989) and K_{SR} channels (Miller, 1982a). The shifted *i*-V curves in this work resemble the results in these reports.

Permeant ion blockade: dose dependence and the role of ion mass

The *i*-V curves in Fig. 8 *A* were calculated from Eq. 14. The parameters used here are identical with those for one ion species except that δ and μ are 0.7 and 0.25, respectively. The solid line represents the control in symmetrical 300-mM K^+ solutions. The *i*-V curves from the top (in the first quarter of the plot) are derived by substituting 0, 50, 150, and 300 mM Rb^+ in side 2, respectively. Both inward and outward currents are reduced by the substitution of Rb^+. The blockage of outward current is proportional to the amount of Rb^+ in side 2. The reduction of inward current differs from that of outward in showing a "saturation." The combination of the reduced outward current and, to a lesser degree, the reduced inward current shifts the *i*-V curve toward a more positive direction. These results resemble the blockage of K^+ current by Rb^+ in K_{Ca} and K_{DR} channels (Eisenman et al., 1986; Clay, 1983). The Rb^+ blockade is closely related to the distinction of ion masses between K^+ and Rb^+. Compared with that of K^+, the water–ion mass fraction of Rb^+ is small. The depth of the energy

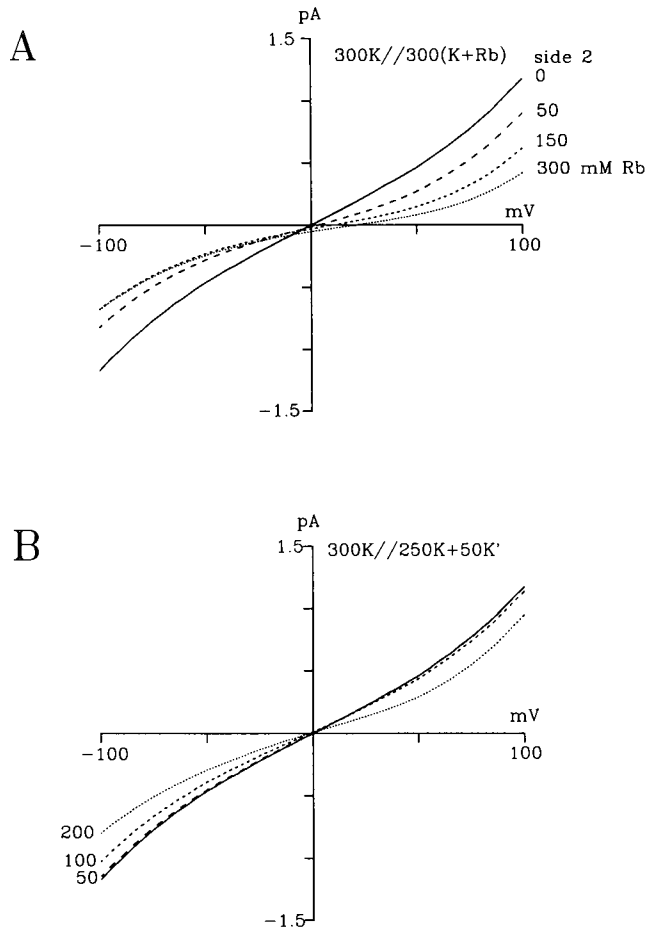

FIGURE 8 (*A*) The dose and voltage dependence of the blockade by the permeant ion Rb^+. The solid *i*-V curve is the control in symmetrical 300-mM K^+ solutions. K^+ is substituted by Rb^+ in side 2 whose dosages are labeled in the plot. (*B*) Blocking effects of 50 mM of the heavy K^+ (K'^+), which have an ion radius identical to K^+ but different ion masses as indicated in the third quarter of the plot.

well of Rb^+ is effectively increased by this lower water–ion mass fraction. The long dwell time of Rb^+ at the binding site blocks the traffic of K^+ translocations. By an increase in Rb^+ substitution in side 2, Rb^+ in the solution has more chance to knock off other Rb ions, which results in an increase in the rate of the dissociation of bound Rb^+ to side 1. To demonstrate this point of view explicitly, similar *i*-V curves in Fig. 8 *B* were calculated in the presence of a hypothetical heavy K^+ (K'^+), which substitutes for 50 mM K^+ in side 2. This ion has the same radius as K^+, but the mass was varied from 50 to 200 g/mol. The identical radius of K^+ and K'^+ results in a matching energy profile for these two ion species. The blockade of current in this plot, therefore, is due purely to the effect of the different ion masses. The solid line is again the control in symmetrical 300-mM K^+ solutions. The potency of this hypothetical K'^+ blockade increases as the ion masses of two ion species become more distinct. The reversal potential for K'^+ blockade shifts slightly to the negative direction. This results from a higher ion mass of K'^+ that reduces its average speed, thus decreasing the on-rate of K'^+ and the inward current. For Rb^+, although its higher ion mass reduces the average speed, its larger ion radius decreases the dehydration barrier, resulting in a higher on-rate. Therefore, to shift the reversal potential toward a more positive direction, the test ions (Rb^+ here) must have both higher ion mass and slightly larger ion radius than that of the reference ions (K^+ here).

Permeant ion blockade: reversal potentials are activity dependent

The inset of Fig. 9 depicts an *i*-V curve in which 300 mM K^+ and 300 mM Tl^+ are placed on side 1 and side 2 of the channel, respectively. Reversal potentials in Fig. 9 were obtained from such *i*-V curves in which the activities of both sides were simultaneously changed. The reversal potential increases steeply from 0 to 16 mV and reaches a plateau beyond 200 mM. The molecular mechanism for the elevation of reversal potential again involves the ion–ion and the water–ion interactions as described in the Theory section. Since Tl^+ stays longer at the binding site, its dissociation dominantly determines reversal potential. The most effective ions to knock off the bound Tl^+ are those of their own kind in side 2. The consequence of increasing Tl^+ activity at this side is to

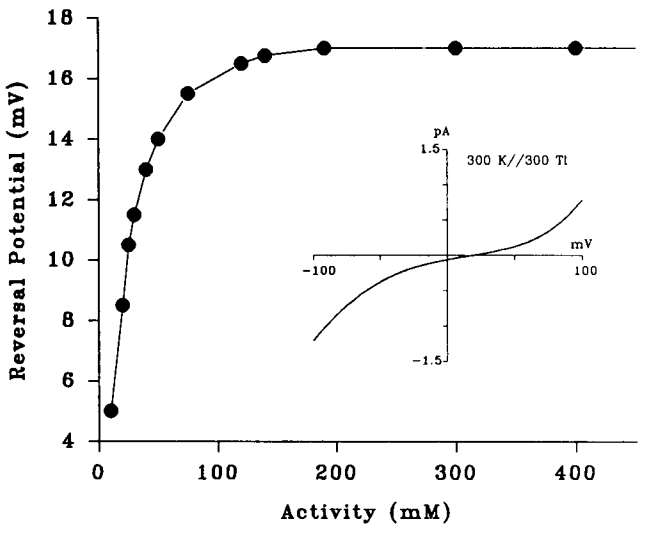

FIGURE 9 Activity-dependent reversal potentials. K^+ salt is placed in side 1 and Tl^+ is placed in side 2. (*Inset*) A sample *i*-V curve shows a positive reversal potential, where 300 mM K^+ is in side 1 and 300 mM Tl^+ in side 2.

increase the knock-off rate of Tl^+ to the *trans* side, resulting in elevations of inward current. Therefore, the reversal potential becomes more positive. The results shown here are consistent with the results in GA channels (Myers and Haydon, 1972).

Permeant ion blockade: anomalous mole-fraction behavior

The calculated anomalous mole-fraction effects on NH_4^+, Rb^+, and Tl^+ mixed with K^+ are shown in Fig. 10. The parameters in Table 2 and Eq. 14 were used. It has been suggested that NH_4^+ forms hydrogen bonds with the selectivity filter (Hille, 1975). The effective radius of NH_4^+ appears to be significantly less than its crystal radius of 1.43 Å (Weast et al., 1989; Villarroel et al., 1991). In this work, the ion radius of NH_4^+ was varied to simulate the experimental results. The data shown in Fig. 10 were obtained when this radius equals 1.32 Å. Because the *i*-V curves are symmetrical and cross the origin, the cord conductances calculated at 1 mV are very close to the zero voltage slope conductance. The curves shown in the graph are consistent with the results in K_{DR} channels (Wagoner and Oxford, 1987) in the following two aspects. First, the steepness of X^+ blocking K^+ is in the order: $Tl^+ > Rb^+ > NH_4^+$, which corresponds to the order of ion masses. Second, they show a minimum in conductance, NH_4^+ at 210 mM, Tl^+ at 120 mM; for Rb^+ it is marginal (at 210 mM Rb^+). This agreement confirms the predicted effects for ion–ion and water–ion interactions, i.e., the higher the ion mass of X^+ the more potently it blocks K^+ current. Not only do the heavier ions stay at the binding site longer, it is also harder to knock them off with K^+. The rising phase of the conductance at higher concentrations of X^+ suggests that when entering X^+ are similar to bound X^+, unblocking is more effective.

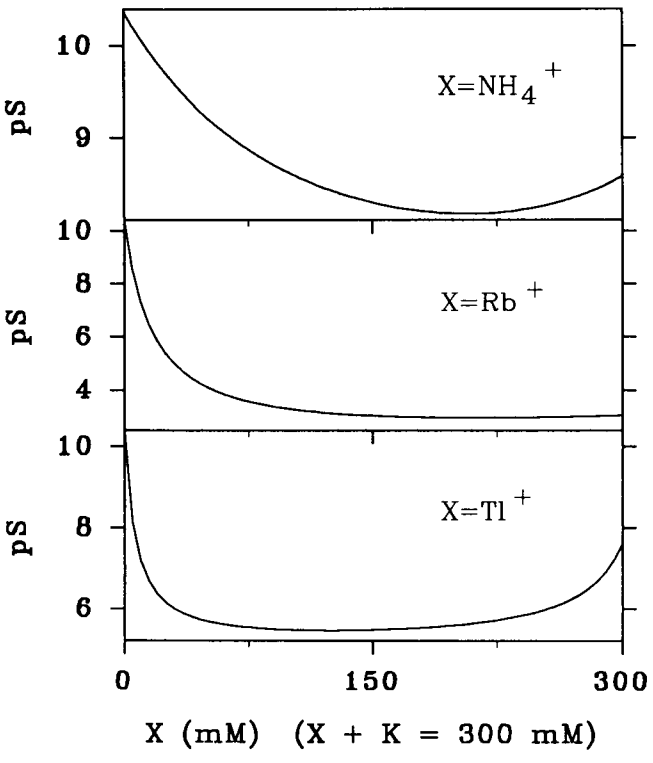

FIGURE 10 The mole fraction behaviors of Rb^+, Tl^+, and NH_4^+ mixed with K^+. The chord conductances were calculated at 1 mV.

DISCUSSION

The following permeation behaviors: (*a*) super- and subsaturations, (*b*) a flux-ratio exponent > 1, (*c*) activity-dependent reversal potentials, and (*d*) the anomalous mole-fraction effect, have been widely accepted as evidence and then structural criteria for multi-ion occupancy in multi-site channels (Finkelstein and Andersen, 1981). In this work, these phenomena are shown as the characteristics of ion–ion and water–ion interactions in a single-site channel. This difference between the current theory and the Eyring rate theory originates from the treatment of ion–ion and water–ion knock-off interactions. In Eyring rate theory, the binding of two or more ions in a channel simultaneously is a prerequisite for ion–ion interactions. These ions then have to be held by two or more physical binding sites. Constrained by long range repulsions, the channel also must be long enough to accommodate these binding sites. Conversely, the current approach treats those interactions directly according to Newton's dynamic laws. The essential assumption is that the entering ions and local water molecules can knock off the bound ion. The occurrence of these interactions requires that the distance between the entering ions and the bound ion is shorter than the range of Columbic interactions. Depending on the length of the tunnel, the occupancy that permits these interactions could be single, transient double, permanent double, etc. Thus, the presence of these interactions does not strictly rely on the occupancy, the number of the binding sites, and the length of tunnels. It is concluded from this analysis that "multi-ion permeation behaviors" may be caused by ion–ion and water–ion knock-off interactions in channels; the presence of these interactions does not require two or more binding sites in a channel. This conclusion suggests that these interactions may also be present in channels that have not yet been proposed as multi-ion channels. This prediction is supported by the super- and subsaturation effects seen in AchR (Dani and Eisenman, 1984, 1986) and K_{SR} chan-

nels (Coronado et al., 1980), water-streaming in AchR (Dani, 1987) and K_{SR} channels (Miller, 1982a), and also the anomalous mole-fraction behavior in K_{SR} channels (Fox, 1983). Therefore, using those permeation behaviors as the criteria to justify the number of binding sites in a channel is questionable.

The studies of intra-channel structure and its energy profiles have long been influenced by known properties of enzymes and the use of Eyring rate theory. The most commonly proposed channel structure includes a series of charged or polar groups along the channel interior that form multiple energy minima or binding sites. Between pairs of these energy minima, barriers are created for ions to hop from one site to another. This view of a channel can be characterized as a "binding-derived energy profile." Along with the description of the selectivity filter, Hille (1975) proposed that the geometry of channels provides physical hindrance, thus modifying the barriers of energy profiles. This "geometry-derived energy profile" was developed further in recent work (Wu, 1991), in which a dehydration process in the vicinity of the selectivity filter was proposed to generate important dehydration energy barriers required for selectivity. The charge at the selectivity filter is important to reduce the dehydration barrier. In this work, the energy encountered by permeant ions is localized in the selectivity filter region; to describe the flux ratio exponent >2, a long tunnel was assumed to hold one or more ion(s). It is desirable, then, to extend the "geometry-derived energy profile" to describe the possible energy barriers in the tunnel. Assume that the outer most hydration layer of the ion needs to be substituted by the tunnel lining in order for ions to enter the tunnel; and the inner hydration layer of the ion has to be removed to allow the almost naked ion to pass through the selectivity filter. Then, the ion must encounter an energy barrier for the initial dehydration at the entrance of the tunnel and the second dehydration energy barrier adjacent to the selectivity filter. If the energy minimum between those two barriers is defined as a "tunnel site," then for impermeant inorganic ions, there are two such sites at each side of the selectivity filter. Constrained by Columbic repulsions, the maximum number of ions that are allowed to stay in one tunnel may be determined by the length of the tunnel. For ions that can pass through a channel, the polar or charged selectivity filter may behave as an additional binding site. This view suggests that there are at least two energy minima for small impermeant ions, and an additional one for permeant ions in a real channel. If the length of the tunnel is shorter than the distance of effective Columbic interactions between the ions in the channel, the entering ion may be able to knock off the bound ion without deeply entering the tunnel. The ion–ion interactions discussed in this work are more suited to these channels. For a channel with long tunnels, the entering ion(s) might have to dwell at a tunnel site before knocking off the bound ion. This work provides a preliminary treatment for applying dynamic interaction theory to explain a flux ratio exponent >2 when more than one ion stays in a long tunnel.

The analysis in this study has also been able to specify which knock-off mechanism participates in these permeation behaviors. Supersaturation and a flux-ratio exponent >1 are the results of ion–ion knock-off interactions. Subsaturation, half-saturation activities, and water-streaming currents are related to water–ion knock-off interactions. Both knock-off mechanisms are involved in activity-dependent reversal potentials and anomalous mole-fraction behavior. Furthermore, the extent of these phenomena is found to be linked to two major parameters, the energy transmission factor, and the mass fraction of two interacting molecules. The former is likely to be determined primarily by channel structure. The latter is an ion species-dependent parameter; i.e., the greater the difference in ion masses between the interacting particles, the less energy can be transferred. In water–ion interactions, the water–ion mass fraction is determined by the ion mass. Ions of higher mass are less likely to be knocked off from the binding site, which leads to a higher apparent affinity. The concept of ion mass being a major determinant in ion–ion and water–ion interactions results directly from the dynamic approach used in this analysis. The predictions from this model are, in general, consistent with published experimental results.

There are three adjustable parameters that are introduced to match empirical findings. The mass-independent constant c in water–ion interactions is used to match the experimentally determined selectivity of Tl^+ and Rb^+ with respect to that of K^+. If c is zero, then the conductances of these two ion species appear too low. A more in-depth consideration relates to the different types of dynamic interactions. Ion–ion collisions result from purely electrostatic repulsion occurring over a long distance. However, when a water molecule moves toward the ion, it is attracted at a distance and then repelled by short range interactions when they are close together. Introducing c into the term of water–ion interactions seems to be a reasonable and simple way to account for this difference. The weakest part of this work is that the ionic partition coefficients f_A and f_B were chosen to be ion-mass dependent ($f_i = (m_i/250)^{1/3}$, $i = A, B$). This choice is made solely to simulate the experimental result of the anomalous mole-fraction effect shown in Fig. 11. The three curves correspond to $z = 0$, ⅓, and ½, respectively (z = the exponent of $m_i/250$). If f_i is independent of ion mass (when $z = 0$),

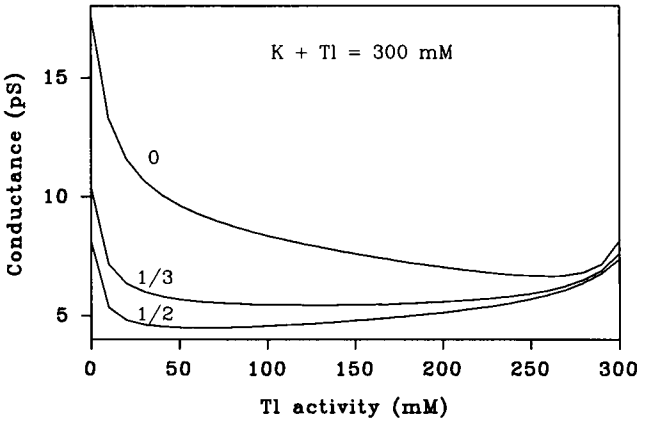

FIGURE 11 The dependence of conductance on the mole fraction of K^+ and Tl^+ mixture where z = 0, ⅓, and ½, respectively ($f_i = (m_i/250)^z, i = K^+, Tl^+$).

the conductance minimum is too close to the high Tl^+ fraction, and the lighter ion species blocks the current steeply at its low mole fraction. Such behaviors are inconsistent with the experimental results (Eisenman et al., 1986; Wagoner and Oxford, 1987). An ion-mass dependent f_i (where $z = ⅓$) significantly relieves this inconsistency. This coefficient can be interpreted in terms of either the ionic dilution or the reduction of average ionic speed within channels. Both reductions are more significant for the lighter ion species. The interactions exerted by the lipid membrane and channel wall, e.g., image potentials, are likely to be the causes for these reductions. The repulsions exerted by the bound ion(s) in channels also might be responsible. The mechanism by which these reductions depend on ion mass remains unclear. The parameters, δ, μ, c, f_W, f_A, f_B, and h are not independent of each other, it is difficult to interpret their magnitude rigorously.

The predictions derived from the present analysis are summarized as follows.

(*a*) The saturation behavior of ion channels may, but generally does not, follow the Michaelis-Menten relation. It consists of two components: supersaturation and subsaturation. The former is determined by ion–ion knock-off interactions and appears to be prominent when the channel is short. The latter is related to the number of water molecules available in the channel and is prominent when the tunnel is long and polar, and also when the ion radius is larger. The half-saturation activity is primarily determined by the water–ion mass fraction. For two ion species with the same radii and masses larger than that of water molecules, the heavier ion species exhibits higher apparent affinity.

(*b*) Water-streaming current is the consequence of imbalanced water–ion knock-off interactions. For a pair of charge carriers with similar radii, this effect is expected to be more prominent when the ion mass is closer to the mass of a water molecule.

(*c*) The flux-ratio exponent can be >1 even for a channel with a single binding site and with a short tunnel; but it is unlikely to exceed 1.4 unless the tunnel is long enough to hold one or more ion(s) most of the time.

(*d*) In biionic solutions containing two permeant ion species that have similar radii but different masses, the reversal potential is activity dependent. In contrast to that in symmetrical solutions, the flux of the heavier ion species may be larger than that of lighter ones in a wide range of solute activities.

(*e*) When two permeant ion species are mixed in solution, the presence of a fraction of either ion species blocks the current carried by the other ion species and facilitates the permeation of the ions of their own kind. The blockade by the heavier ions is likely to be more potent than that of the lighter ones.

APPENDIX

If $m_B \gg m_A$, after an entering ion B knocks off the bound ion A at O, it is possible that the ion B has enough residual velocity to pass over the dehydration barrier, W_{B10} or W_{B20}, resulting in the transition from OA to OB. The following state diagram includes this transition:

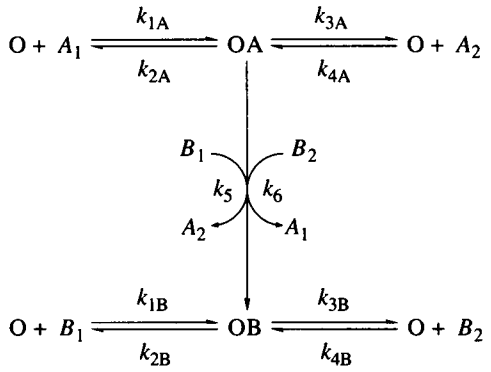

The corresponding flux equation is:

$$j = \frac{\begin{aligned}&(k_{2B}+k_{3B})[(k_{3A}+k_5B_1)k_{1A}A_1-(k_{2A}+k_6B_2)k_{4A}A_2]\\&+(k_{3B}k_5B_1-k_{2B}k_6B_2)(k_{1A}A_1+k_{4A}A_2)\\&+(k_{2A}+k_{3A}+k_5B_1+k_6B_2)(k_{3B}k_{1B}B_1-k_{2B}k_{4B}B_2)\end{aligned}}{\begin{aligned}&(k_{2B}+k_{3B}+k_5B_1+k_6B_2)(k_{1A}A_1+k_{4A}A_2)\\&+(k_{2A}+k_{3A}+k_5B_1+k_6B_2)(k_{2B}+k_{3B}+k_{1B}B_1+k_{4B}B_2)\end{aligned}}. \quad (24)$$

In case of a mixture of Tl^+ and K^+, the translation rate of Tl^+ is 10^6–10^8/s. k_5 or k_6, however, is usually less than 10^2–10^3/s. Disregarding these transitions markedly simplifies the formulation and has an insignificant effect on channel permeation behavior discussed in this work. When $m_A = m_B$ (only one permeant ion species), the rate of this transition is expected to be even less.

I am greatly indebted to Dr. P. Shrager for encouragement, critical comments, and wording on this work, and to V. Roth for proofreading of the manuscript.

This work was supported by grant RG-1774 from the National Multiple Sclerosis Society and grant NS-17965 from the National Institutes of Health to P. Shrager.

Received for publication 22 July 1991 and in final form 2 January 1992.

REFERENCES

Alcayaga, C., X. Cecchi, O. Alvares, and R. Latorre. 1989. Streaming potential measurements in Ca^{++}-activated K^+ channels from skeletal and smooth muscle. *Biophys. J.* 55:367–371.

Almers, W., and E. W. McCleskey. 1984. The non-selective conductance in calcium channels of frog muscle: calcium selectivity in a single-file pore. *J. Physiol. (Lond.).* 353:585–608.

Barnes, G. 1958. Study of collisions. *Am. J. Phys.* 26:5–12.

Begenisich, T., and D. Busath. 1980. Sodium flux ratio in voltage-clamped squid giant axons. *J. Gen. Physiol.* 77:489–502.

Begenisich, T., and P. De Weer. 1980. Potassium flux ratio in voltage-clamped squid giant axons. *J. Gen. Physiol.* 76:83–98.

Bezanilla, F., and C. M. Armstrong. 1972. Negative conductance caused by entry of sodium and cesium ions into the potassium channels of squid axons. *J. Gen. Physiol.* 60:588–608.

Bormann, J., O. P. Hamill, and B. Sakmann. 1987. Mechanism of anion permeation through channels gated by glycine and γ-aminobutyric acid in mouse cultured spinal neurones. *J. Physiol. (Lond.).* 385:243–286.

Cajori. F. 1934. Newton's Principa—A Revision of Mott's Translation. University of California Press, Berkeley, CA. 18 pp.

Cecchi, X., R. Bull, R. Franzoy, R. Coronado, and O. Alverez. 1982. Probing the pore size of the hemocyanin channel. *Biochim. Biophys. Acta.* 693:173–176.

Chandler, W. K., and H. Meves. 1965. Voltage clamp experiments on internally perfused giant axons. *J. Physiol. (Lond.).* 180:788–820.

Clay, J. R. 1983. Effects of external cesium and rubidium on outward potassium currents in squid axons. *Biophys. J.* 42:43–53.

Cleland, W. W. 1970. Steady state kinetics. *In* The Enzymes. Vol. II. P. D. Boyer, editor. Academic Press, New York. 1–65.

Correa, A. M., R. Latorre, and F. Benzanilla. 1991. Ion permeation in normal and batrachotoxin-modified Na^+ channels in the squid giant axon. *J. Gen. Physiol.* 97:605–625.

Coronado, R., R. L. Rosenberg, and C. Miller. 1980. Ionic selectivity, saturation, and block in a K^+-selective channel from sarcoplasmic reticulum. *J. Gen. Physiol.* 76:425–446.

Dani, J. A., and G. Eisenman. 1984. Acetylcholine-activated channel. Current-voltage relations in symmetrical Na^+ solutions. *Biophys. J.* 45:10–12.

Dani, J. A. 1987. Streaming potential measurements indicate the narrowest cross section of the nicotinic acetylcholine receptor pore is very short. *Biophys. J.* 51:395*a*. (Abstr.)

Eisenman, G., J. Sandblom, and E. Neher. 1978. Interactions in cation permeation through the gramicidin channel. Cs, Rb, K, Na, Li, Tl, H, and effects of anion binding. *Biophys. J.* 22:307–340.

Eisenman, G. R. Latorre, and C. Miller. 1986. Multi-ion conductance and selectivity in the high-conductance Ca^{++}-activated K^+ channel from skeletal muscle. *Biophys. J.* 50:1025–1034.

Finkelstein, A., and O. S. Andersen. 1981. The gramicidin A channel: a review of its permeability characteristics with special reference to the single-file aspect of transport. *J. Membr. Biol.* 59:155–171.

Fox, J. A. 1983. Thallous ion permeation through the cation-selective channels of the Sarcoplasmic reticulum. *Biochim. Biophys. Acta.* 736:241–245.

Green, W. N., L. B. Weiss, and O. S. Andersen. 1987. Batrachotoxin-modified sodium channels in planar lipid bilayers. Ion peameation and block. *J. Gen. Physiol.* 89:841–872.

Hagiwara, S., S. Miyazaki, S. Kranse, and S. Ciani. 1977. Anomalous permeabilities of the egg cell membrane of a starfish in K^+-Tl^+ mixtures. *J. Gen. Physiol.* 70:269–281.

Hals, G. D., P. G. Stein, and P. T. Palade. 1989. Single channel characteristics of a high conductance anion channel in "saroballs." *J. Gen. Physiol.* 93:385–410.

Heckmann, K. 1972. Single-file diffusion. *In* Biomembranes: Passive Permeability of Cell Membranes. Vol. 3. F. Kreuzer and J. F. G. Slegers, editors. Plenum Press, New York. 127–153.

Hess, P., J. B. Lansman, and R. W. Tsien. 1986. Calcium channel selectivity for divalent and monovalent cations. *J. Gen. Physiol.* 88:293–319.

Hess, P., and R. W. Tsien. 1984. Mechanism of ion permeation through calcium channels. *Nature (Lond.).* 309:453–456.

Hill, J. A., R. Coronado, and H. Strauss. 1989. Potassium channel of cardiac sarcoplasmic reticulum is a multi-ion channel. *Biophys. J.* 55:35–46.

Hille, B. 1975. Ion selectivity of Na and K channels of nerve membranes. *In* Membranes. G. Eisenman, editor. Marcel Dekker, New York. 3:255–323.

Hille, B., and W. Schwarz. 1978. Potassium channels as multi-ion single-file pores. *J. Gen. Physiol.* 72:409–442.

Hille, B., and W. Schwarz. 1979. K channels in excitable cells as multi-ion pores. *Brain Res. Bull.* 4:159–162.

Hille, B. 1984. Ionic Channels of Excitable Membranes. Sinauer Associates Inc., Massachusetts. 255 pp.

Hladky, S. B., and D. A. Haydon. 1972. Ion transfer across lipid membranes in the presence of gramicidin A. *Biochim. Biophys. Acta.* 274:294–312.

Hodgkin, A. L., and A. F. Huxley. 1952. Currents carried by sodium and potassium ion through the membrane of the giant axon of *Loligo. J. Physiol. (Lond.).* 116:448–472.

Hodgkin, A. L., and R. D. Keynes. 1955. The potassium permeability of a giant nerve fibre. *J. Physiol. (Lond.).* 128:61–68.

Horn, R., and J. Patlak. 1980. Single channel currents from excised patches of muscle membrane. *Proc. Natl. Acad. Sci. USA.* 77:6930–6934.

Kostyuk, P. G., and O. A. Krishtal. 1977. Separation of sodium and calcium currents in the somatic membrane of molluscan neurones. *J. Physiol. (Lond.).* 270:545–568.

Lansman, J. B., P. Hess, and R. W. Tsien. 1986. Blockade of current through single calcium channels by Cd^{2+}, Mg^{2+}, and Ca^{2+}. *J. Gen. Physiol.* 88:321–347.

Latorre, R., and O. Alvarez. 1981. Voltage-dependent channels in planar lipid bilayer membranes. *Physiol. Rev.* 61:77–150.

Libuś, Z. 1990. Quantitative determination of ion-water interactions from water activity and density data. *Zeitschrift für Physikalische Chemie Neue Folge, Bd.* 166:S71–78.

Miller, C. 1982a. Coupling of water and ion fluxes in a K^+-selective channel of sarcoplasmic reticulum. *Biophys. J.* 38:227–230.

Miller, C. 1982b. *Bis*-quaternary ammonium blockers as structural probes of the sarcoplasmic reticulum K^+ channel. *J. Gen. Physiol.* 97:869–891.

Myers, V. B., and D. A. Haydon. 1972. Ion transfer across lipid membranes in the presence of gramicidin A. II. The ion selectivity. *Biochim. Biophys. Acta.* 274:313–322.

Robinson, R. A., and R. H. Stokes. 1955. Electrolyte Solutions. Butterworths Scientific Publications, London. 479 pp.

Spalding, B. C., O. Senyk, J. Swift, and P. Horowicz. 1981. Unidirectional flux ratio for potassium ions in depolarized frog skeletal muscle. *Am. J. Physiol.* 241:C68–C75.

Urry, D. W. 1971. The gramicidin A transmembrane channel: a proposed $\pi_{(L,D)}$ helix. *Proc. Natl. Acad. Sci. USA.* 68:672–676.

Vergara, C., E. Moczydłowski, and R. Latorre. 1984. Conduction, blockade and gating in a Ca^{++}-activated K^+ channel incorporated into planar lipid bilayers. *Biophys. J.* 45:73–76.

Villarroel, A., S. Herlitze, M. Koenen, and B. Sakmann. 1991. Location of a threonine residue in the α-subunit M2 transmembrane segment that determines the ion flow through the acetylcholine receptor channel. *Proc. R. Soc. Lond. B.* 243:69–74.

Wagoner, P. K., and G. S. Oxford. 1987. Cation permeation through the voltage-dependent potassium channel in the squid axon. Characteristics and mechanisms. *J. Gen. Physiol.* 90:261–290.

Weast, R. C., D. L. Lide, M. J. Astle, and W. H. Beyer. 1989. CRC Handbook of Chemistry and Physics. CRC Press, Inc., Boca Raton, Florida.

Wu, J. 1991. Microscopic model for selective permeation in ion channels. *Biophys. J.* 60:238–251.

Yellen, G. 1987. Permeation in potassium channels: implications for channel structure. *Annu. Rev. Biophys. Biophys. Chem.* 16:227.

Yellen, G., M. E. Jurman, T. Abramson, and R. Mackinnon. 1991. Mutations affecting internal TEA blockade identify the probable pore-forming region of a K^+ channel. *Science (Wash. DC).* 251:939–942.